Nuclear Instruments and Methods in Physics Research A 743 (2014) 22–29

Contents lists available at ScienceDirect

Nuclear Instruments and Methods in Physics Research A

journal homepage: www.elsevier.com/locate/nima

Calibration and performance of the AMS-02 time of flight detector in space

V. Bindi [a], G.M. Chen [b], H.S. Chen [b], E. Choumilov [c], V. Choutko [c], A. Contin [d,e], A. Lebedev [c], Y.S. Lu [b], N. Masi [d,e], A. Oliva [f], F. Palmonari [d,e], L. Quadrani [d,e], Q. Yan [b,*]

[a] University of Hawaii, Physics and Astronomy Department, 2505 Correa Road, WAT 432, Honolulu, HI 96822, USA
[b] Institute of High Energy Physics, IHEP, Chinese Academy of Sciences, Beijing 100049, China
[c] Massachusetts Institute of Technology, MIT, Cambridge, MA 02139, USA
[d] Universit'a di Bologna, I-40126 Bologna, Italy
[e] INFN-Sezione di Bologna, I-40126 Bologna, Italy
[f] Centro de Investigaciones Energeticas, Medioambientales y Tecnologicas, CIEMAT, E-28040 Madrid, Spain

ARTICLE INFO

Article history:
Received 13 October 2013
Received in revised form
24 December 2013
Accepted 4 January 2014
Available online 11 January 2014

Keywords:
AMS
TOF
Scintillator
Calibration
Charge
Velocity

ABSTRACT

AMS-02 is a high energy particle detector deployed in May 19, 2011 on board of the International Space Station (ISS) where it is expected to be in operation for the ISS lifetime of at least a decade. The main goal of AMS-02 is the detection of cosmic rays and gammas from the GeV to the TeV energy region to search for anti-matter, dark matter and understanding the origin of the cosmic rays. The AMS-02 time of flight (TOF) detector provides the trigger to experiment and allows precise measurements of the cosmic rays velocity and charge magnitude from hydrogen to iron and above. With the data set acquired during the first two and a half years of operation in space, a precise time-dependent calibration for time, velocity and charge measured by the TOF had been developed. The TOF calibration methods are described and the AMS-02 TOF performance in space is presented.

1. Introduction

The TOF system of AMS-02 [1] provides an accurate measurement of the velocity and of the charge magnitude of the detected cosmic rays (CRs). The detector was designed to ensure long term reliability, thanks to the choice of components and their redundancy. During the first two and a half years of operation in space, TOF operated according to the design, providing the trigger to the AMS-02 detector with an efficiency approaching 100%. In order to exploit the full potential of the instrument in a constantly changing thermal environment, a time-dependent calibration method of TOF system was developed.

2. The AMS detector

The layout of the AMS-02 detector [2] is shown in Fig. 1. AMS-02 consists of the following:

- A permanent magnet with a 0.14 T dipole-shaped magnetic field to bend charged particles.
- Nine planes of silicon tracker (Tracker) [3] to reconstruct the particle rigidity[1] (R). With a spatial point resolution of 7 μm ($2 \le Z \le 8$), and a maximum lever arm of about 3 m, the maximum detectable rigidity (MDR) is estimated to be 3 TV for ions. Moreover, each Tracker plane can independently evaluate the charge magnitude of the crossing particle in a wide range ($1 \le Z \le 26$).
- Four layers of time of flight (TOF) counters [4] to provide the trigger and measure the particle velocity and charge.
- A transition radiation detector (TRD) [5] to separate electrons from hadrons at the 10^{-4} level.
- An array of anti-coincidence counters surrounding the inner tracker (ACC) [6] to reject interactions on the magnet bore with an efficiency of 99.99%.
- A ring imaging Cherenkov detector (RICH) [7] to measure the velocity of the crossing particle with a resolution of 0.1% and the absolute charge up to $Z=26$.
- A 17 radiation lengths thick electromagnetic calorimeter (ECAL) [8] to measure the energy released by electromagnetic particles with the resolution of 2% in the hundreds GeV energy region and separate electrons from hadrons at the 10^{-4} level.

* Corresponding author.
E-mail address: qyan@cern.ch (Q. Yan).

[1] The particle rigidity is defined as momentum (P) divided by charge (Z).

0168-9002/$ - see front matter © 2014 Elsevier B.V. All rights reserved.
http://dx.doi.org/10.1016/j.nima.2014.01.002

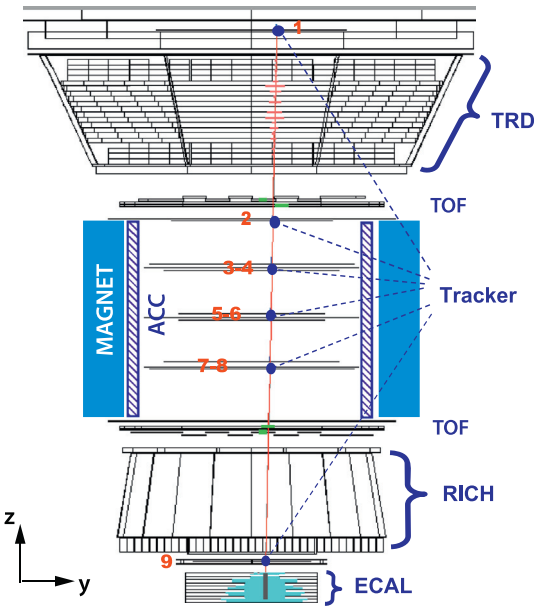

Fig. 1. Schematics of the AMS-02 detector.

3. TOF detector

The AMS-02 TOF system (shown in Fig. 2) had been designed and built at the INFN laboratories in Bologna (Italy). It is composed of four layers of EJ-200 scintillator counters [4] located two above and two below the AMS magnet. The upper TOF (UTOF) plane (layers 0 and 1) is firmly connected to the TRD support structure. The lower TOF (LTOF) plane (layers 2 and 3) is fixed to the Unique Support Structure (USS). The vertical distance between UTOF and LTOF is about 120 cm.

The four TOF layers have 8, 8, 10 and 8 paddles: the internal paddles have a rectangular shape, 1 cm thick, 12 cm width and 110–135 cm length, while the external counters have a trapezoidal shape with 18–26 cm width and 110 cm length. To ensure 100% trigger efficiency, neighbouring counters are overlapped by 0.5 cm. Each side of a TOF counter is connected to 2 or 3 R5946 Hamamatsu Photo-Multiplier Tubes (PMTs) [9] through plexiglass light guides. The light guides can be straight, tilted or twisted to minimize the effect of magnetic field on the PMT signal [10,11]. The 144 photomultipliers, connected to the 34 TOF paddles, are powered by 4 power supply (Scintillator High Voltage, SHV), which can provide a voltage between 1700 V and 2250 V. The nominal gain of the photomultipliers is about 10^6 when powered at 2000 V.

3.1. TOF readout

The PMT anode and third last dynode signals are read out independently, as shown in Fig. 3. The anode signals from the 2 (3) PMTs of the same counter side are summed up and transmitted to the TOF readout electronics module SFET2 (Scintillator Front End Time) [12] for time and anode charge measurement. Each dynode signal is measured individually by the readout electronics module SFEC (Scintillator Front End Charge) [12] and it is used for the measurement of the charge.

The anode signal is divided into two parts. 95% of the signal is used for the time measurement and for the trigger. It is compared to the following three thresholds:

1. a low threshold (LT), set at ~20% of the minimum ionizing Proton (MIP) signal for time measurement;
2. a high threshold (HT), set at ~60% of the MIP signal for $Z \geq 1$ trigger;
3. a super high threshold (SHT), set at ~400% of the MIP signal for $Z \geq 2$ trigger.

When the signal is above the thresholds, the output is sent to a HPTDC [13] to record the time. The time of the fast trigger is also registered and it is used as the reference time in each event.

The remaining 5% of the anode signal is used for the charge measurement. Anode and dynode analog-to-digital converter (ADC) share a common design. The pulse is integrated by an AICPPP chip (shaper analog integrated circuit) [14] and then digitized.

The anode signal is used to measure absolute charge for low Z nuclei ($1 \leq Z \leq 8$), while the dynode extends the charge measurement to higher Z ($Z \geq 3$) particles.

3.2. Performance of the hardware in space

To assess the TOF capability of operating in space, all the components underwent several vacuum, thermal and vibration tests before their integration on the TOF detector. In addition to that, the UTOF and LTOF have been space qualified, passing through strict thermal vacuum and vibration tests at SERMS laboratories [15]. To ensure a long term reliability, a certain degree of redundancy has been implemented in the TOF system: each counter is 4(6)-fold redundant in PMTs, and doubly redundant in powering and read-out electronics. During the first two years of data taking on the ISS, the TOF detector worked as expected without any major issue.

4. TOF velocity measurement

The velocity $v_{\rm par} = \Delta s/\Delta T$ of particle crossing AMS-02 is measured by the TOF using the particle time of flight ΔT between different layers, and the trajectory length Δs given by the Tracker or by the TOF. The TOF velocity measurement is used to determine the particle velocity magnitude[2] (β) and to distinguish upward-going from downward-going particles. In the following sections the time calibration and the longitudinal coordinate calibration are described.

4.1. Time measurement

TOF anode readout electronic SFET2s for the measurement of the particle crossing time, are located in four different S-Crates [12]. Each S-Crate has four different SFET2 boards, each SFET2 serving two different sides from two TOF layers. The measurement of the particle crossing time is based on a 40 MHz clock HPTDC [13] inside each SFET2.

The time-to-digital converter (TDC) bin widths (nominal: 25 ps) are slightly different depending on the individual electronic components. Specific calibration to equalize the TDC bin width of each SFET2 is performed by using a large statistics of cosmic ray particles. Once the calibration for the TDCs' non-linearity is applied, the TDCs are ready to be used for the time measurement.

The principle of the measurement is shown in Fig. 4. The low threshold measured time T_{LT} in each counter side together with the fast trigger time T_{FT} is related to particle crossing time $T_{\rm par}$ through various delays, which depend on light transmission, on cable length and on the signal shape:

$$T_{LT} = T_{FT} - (T_{\rm par} + T_{trans} + T_{del} + T_{slew}) = T_{FT} - \left(T_{\rm par} + \frac{x}{v_c} + T_{del} + f(A)\right) \quad (1)$$

[2] The particle velocity magnitude is defined as velocity ($v_{\rm par}$) divided by light speed (c).

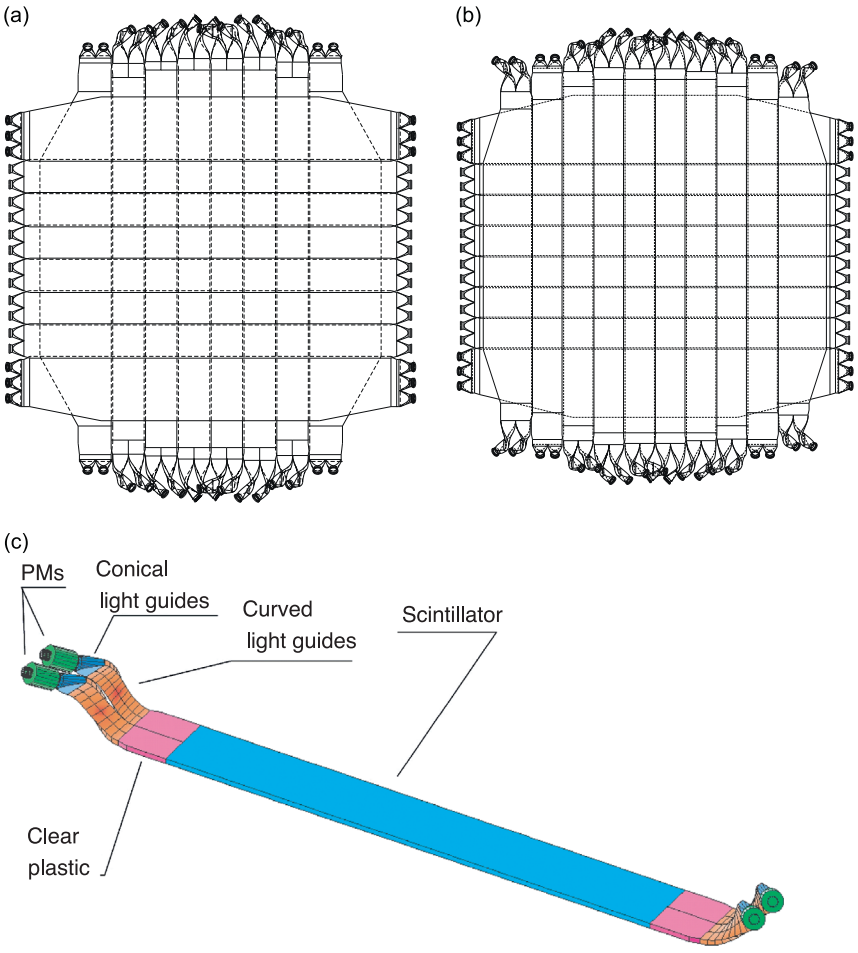

Fig. 2. The TOF detector: (a) upper TOF plane; (b) lower TOF plane; and (c) one counter.

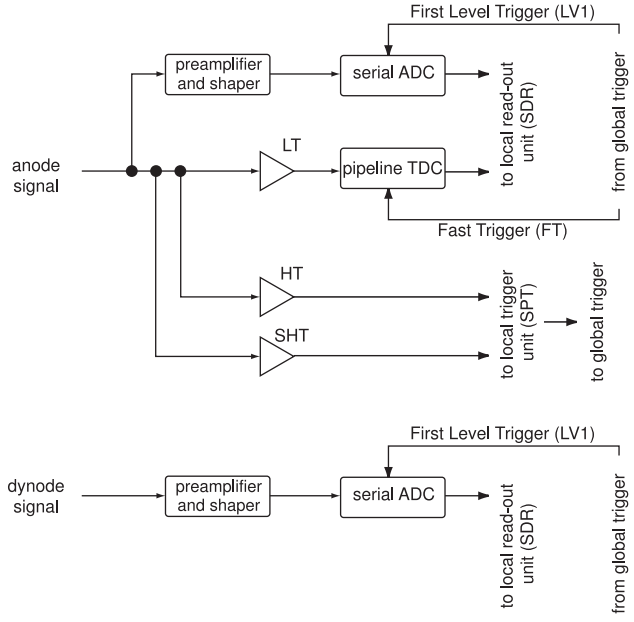

Fig. 3. TOF anode and dynode readout.

where $T_{trans}=x/v_c$ is the light transmission time, T_{del} is the cable and electronics delay time, $T_{slew}=f(A)=S/A^{\gamma}$ is the time walk delay described by the empirical formula, v_c is the effective light speed inside the paddle, A is the anode ADC value, and S and γ are free parameters related to the signal shape.

The particle crossing time $T_{\rm par}$ can be calculated by averaging the measured time $(T_{n,LT}+T_{p,LT})$ from the two counter sides (n and p):

$$T_{n,LT}=T_{FT}-\left(T_{n,\rm par}+\frac{x}{v_c}+T_{n,del}+\frac{S_n}{A_n^{\gamma}}\right) \tag{2}$$

$$T_{p,LT}=T_{FT}-\left(T_{p,\rm par}+\frac{L-x}{v_c}+T_{p,del}+\frac{S_p}{A_p^{\gamma}}\right) \tag{3}$$

to obtain

$$T_{\rm par}=\frac{T_{n,\rm par}+T_{p,\rm par}}{2}=-\frac{T_{n,LT}+T_{p,LT}+\frac{S_n}{A_n^{\gamma}}+\frac{S_p}{A_p^{\gamma}}}{2}-T_{Del}+T_{FT}$$
$$=-T_{np}+T_{FT} \tag{4}$$

where $T_{Del}=(T_{n,del}+T_{p,del}+L/v_c)/2$, and $T_{np}=(T_{n,LT}+T_{p,LT}+S_n/A_n^{\gamma}+S_p/A_p^{\gamma})/2+T_{Del}$. Therefore, each counter has four free parameters, S_n, S_p, T_{Del} and γ, that need to be derived from the data.

4.2. Time calibration

The particle crossing times measured by two different counters c_m and c_k in two different layers l_i and l_j are related to particle velocity $v_{\rm par}$:

$$T_{np(l_ic_m)}-T_{np(l_jc_k)}=-T_{\rm par(l_ic_m)}+T_{\rm par(l_jc_k)}=\frac{L_{l_il_j}}{v_{\rm par}} \tag{5}$$

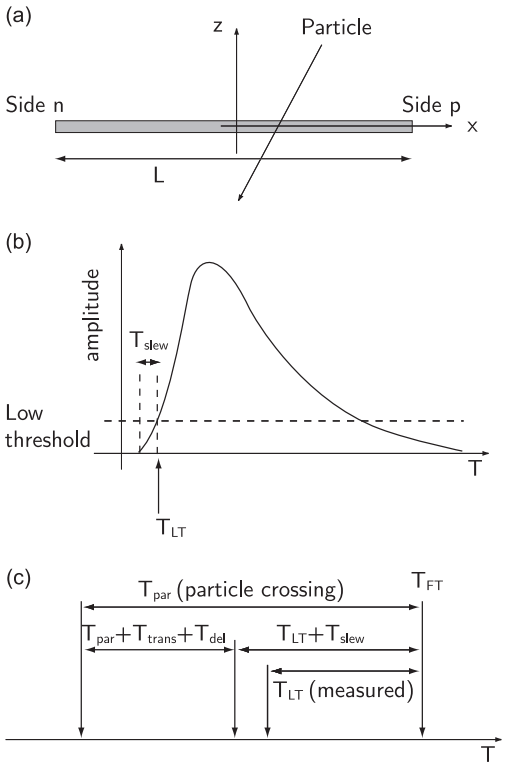

Fig. 4. Principle of the time measurement: particles hitting the counter at position x (a) produce a signal which is discriminated with a low threshold (b); the particle crossing time T_{par} is related to the measured time T_{LT} through various constants (c), as described in the text.

where $L_{l_i l_j}$ is the particle path length between the two TOF layers i and j. $L_{l_i l_j}$ and v_{par} can be obtained from the measurement by the silicon tracker detector.

The time calibration is performed by minimizing the value of the formula, defined as follows:

$$\sum_{l_i l_j} \sum_{c_k c_m} \sum_{\mathrm{events}} \left(T_{np(l_i c_m)} - T_{np(l_j c_k)} - \frac{L_{l_i l_j}}{v_{\mathrm{par}}} \right)^2 \tag{6}$$

where $\sum_{\mathrm{events}}$ sums over all events of the time differences between any two counters in any two TOF layers, $\sum_{c_k c_m}$ sums over all counter pairs in the two layers i and j, and $\sum_{l_i l_j}$ sums over all layer pairs belonging to different planes ($l_0 l_2$, $l_0 l_3$, $l_1 l_2$, $l_1 l_3$).

The 103 time calibration parameters (68 for slewings, 34 for time delays, 1 for γ) for 34 TOF paddles are determined by this minimization.

The calibration of the TOF time measurement is performed using high energy particles with rigidities greater than 20 GV, to ensure that the particle β is close to 1.

The calibration also needs to take into account: the anode gain changes due to the temperature variations, scintillator and PMT ageing and threshold fluctuations. The calibration procedure is thus repeated every 15 days.

The time walk delay $f(A) = S/A^{\gamma}$ is related to the pulse shape, to the LT threshold setting and to the anode amplitude sampling. In order to trace the pulse shapes in the full dynamic range, a sample made of different charged particles (Protons, Heliums and nuclei) with different weights is chosen to perform the calibration.

4.3. Longitudinal coordinate calibration

The difference between the times measured at the two counter sides ($T_{n,LT} - T_{p,LT}$) is related to the coordinate of the hitting point

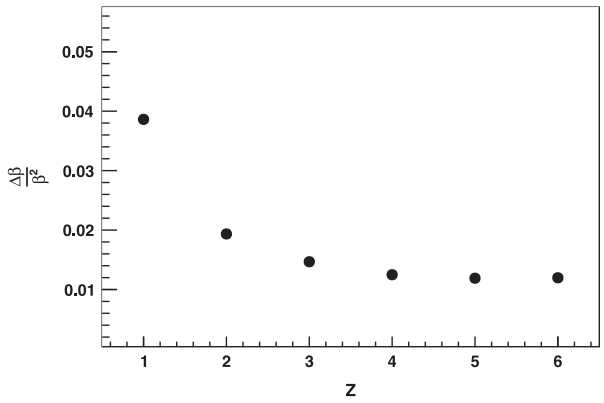

Fig. 5. TOF velocity resolution as a function of the particle charge Z.

of the particle along the counter, C_{TOF}, according to the relation:

$$C_{\mathrm{TOF}} = v_c \frac{\left(T_{n,LT} - \frac{S_n - dS}{A_n^{\gamma}}\right) - \left(T_{p,LT} - \frac{S_p + dS}{A_p^{\gamma}}\right)}{2} + C_0 \tag{7}$$

where S_n, S_p and γ are obtained by the time calibration procedure, dS is a term introduced to balance the change in the effective light speed with amplitude, and C_0 is a constant which takes into account the time differences in the signal transmission due to cable length and electronics.

By matching C_{TOF} with the extrapolation of the Tracker track in the counter, C_{TRACKER}, it is possible to determine, for each counter, the constants v_c, dS and C_0 by minimizing the value of the formula defined as follows:

$$\sum_{\mathrm{events}} (C_{\mathrm{TOF}} - C_{\mathrm{TRACKER}})^2 \tag{8}$$

4.4. Performance in space

In the following, the performance of the TOF system after calibration is described. The data analysed corresponds to the data taking period from July 2011 to May 2013.

The velocity resolution of the TOF system improves with increasing particle charge Z (see Fig. 5) from 4% at $Z=1$ to 1.2% at $Z=6$. Figs. 6 and 7 show the measured β distributions for Helium and Carbon ions, respectively, which correspond to the single counter time resolution is 80 ps for Helium and 48 ps for Carbons.

After the calibration, the resolution on the longitudinal coordinate measured by TOF is about 2.7 cm for Protons and 0.9 cm for Carbon ions, as shown in Fig. 8.

5. TOF charge measurement

The TOF system provides precise measurement of the charge of the particles crossing AMS-02. Several calibration steps are necessary to achieve the best measurement. In the following sections all the calibration corrections are described and the performance of the TOF charge measurement in space is also reported. The relative size of the most important calibration corrections for the TOF charge measurement is shown in Table 1.

5.1. Attenuation and gain calibration

The light generated by the particle in the scintillator is partially absorbed: this effect produces an attenuation of the signal as a function of the particle hit position. This dependence is shown in Fig. 9.

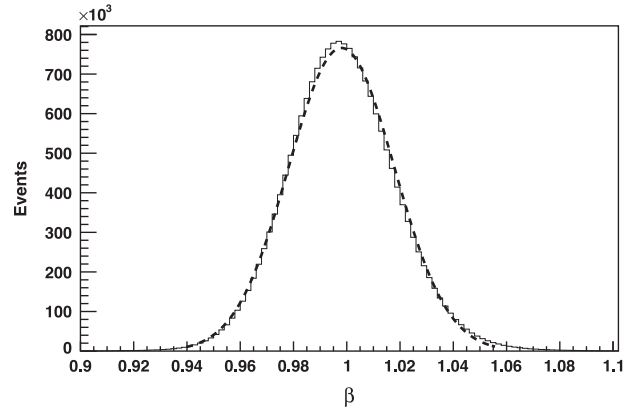

Fig. 6. Measured TOF velocity distribution for Helium ions with $R > 20$ GV. The dashed line is a Gaussian fit with a standard deviation of 2%.

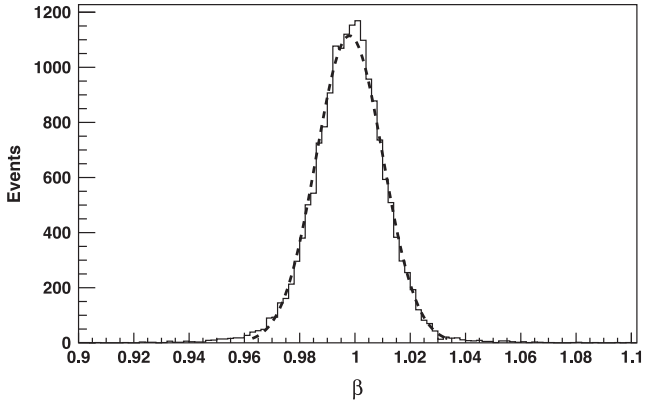

Fig. 7. Measured TOF velocity distribution for Carbon ions with $R > 20$ GV. The dashed line is a Gaussian fit with a standard deviation of 1.2%.

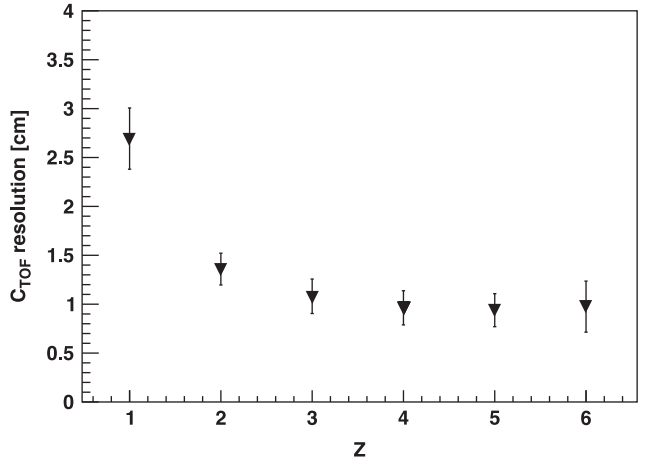

Fig. 8. Average TOF counter longitudinal coordinate resolution as a function of the particle charge Z.

During AMS data acquisition, the signal changes due to varying temperatures, PMT ageing and changing scintillator optical properties. To correct for these effects, a calibration depending on time (i.e. "dynamic") is needed. The dynamic calibration combines scintillator light attenuation properties and PMT gain:

1. For each counter side, the light attenuation calibration is performed every 15 days using anode signals. The calibration sample includes high energy Protons and Helium nuclei. As a result, a function $f_{\mathrm{att}}(x)$ of the hit position is determined for each counter side, to equalize the response along the counter:

$$A_{\mathrm{att}} = \frac{A_{\mathrm{measured}}}{f_{\mathrm{att}}(x)} \tag{9}$$

where A_{att} is the amplitude of the signal corrected for attenuation and A_{measured} is the measured amplitude.

2. For each counter side, the anode gain calibration is performed every 3 days. The calibration sample includes high energy Protons and Helium nuclei. As a result, a gain factor $G_{\mathrm{anode,eq}}$ is determined for each counter side, to equalize all the anode amplitudes:

$$A_{\mathrm{eq}} = \frac{A_{\mathrm{att}}}{G_{\mathrm{anode,eq}}} \tag{10}$$

3. For each PMT dynode, the gain calibration is performed every 7.5 days. The calibration sample includes high energy Carbon nuclei. As a result, a gain factor $G_{\mathrm{dynode,eq}}$ is determined for each PMT to equalize all the dynode amplitudes:

$$D_{\mathrm{eq}} = \frac{D_{\mathrm{att}}}{G_{\mathrm{dynode,eq}}} \tag{11}$$

Fig. 10 shows the light yield corrected for attenuation, obtained after applying the dynamic calibration procedure to one counter side.

After the dynamic calibration, the resulting amplitudes of dynodes and anodes have to be further corrected for saturation, electronics non-linearities and particle velocity using the fully available statistics. These corrections, which do not change with time (i.e. they are "static"), are described in the following sections.

Table 1
TOF charge measurement calibration corrections relative size.

Correction item	Relative amplitude correction
Attenuation	Up to 50% depending on the hit position along the counter
Anode and dynode gain	Up to 5% depending on the PMT temperature
Light yield saturation	$< 4\%$ ($Z \leq 3$) to 150% ($Z = 26$)
Anode non-linearity	$< 1\%$ ($Z \leq 3$) to 100% ($Z = 10$)
Velocity dependence	$< 1\%$ ($\beta = 0.99$) to 150% ($\beta = 0.4$)

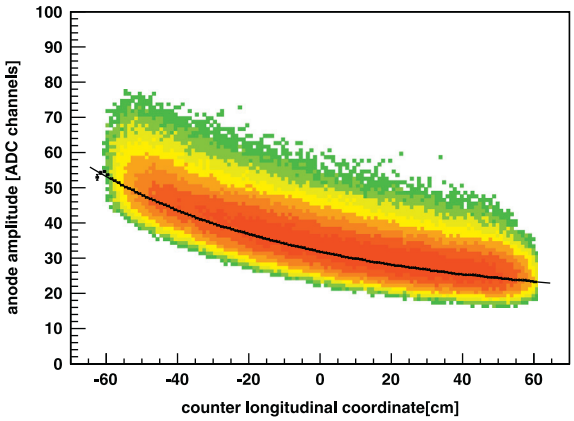

Fig. 9. Anode amplitude measured at one counter side as a function of the longitudinal coordinate of the particle hit point.

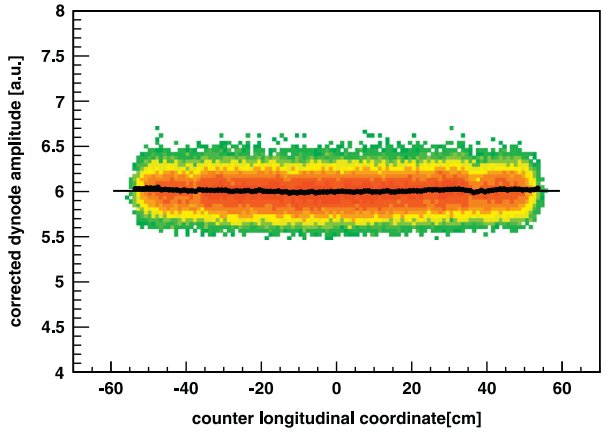

Fig. 10. Dynode amplitude measured for Carbon at one counter side as a function of the longitudinal coordinate of the particle hit point, after the dynamic correction described in the text.

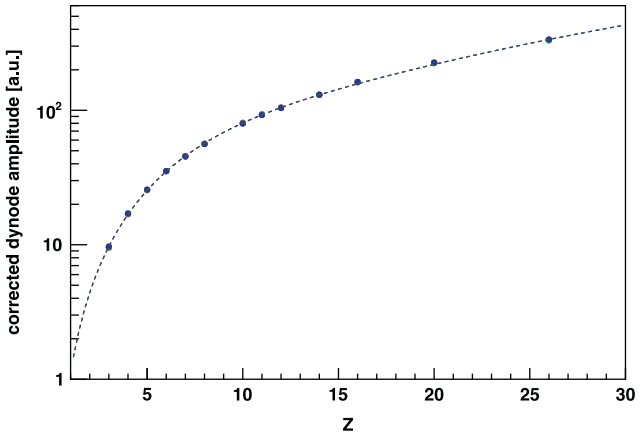

Fig. 11. Measured dynode amplitude, corrected for attenuation, as a function of the particle charge. The solid line is the fit with formula (12).

5.2. Light yield saturation

The scintillation light produced by a high Z particle is not linearly proportional to the energy deposition. The number of emitted photons tends to saturate with increasing deposited energy (dE/dx). This effect is known as Birks' saturation [17].

The saturation has been parametrized with the following formula (Fig. 11):

$$\frac{dE}{dx}=\frac{aZ^2}{1+b\ \arctan\left(\frac{c}{b}Z^2\right)} \tag{12}$$

where a, b and c are constant parameters, and Z is determined using the Tracker charge measurements. For $Z\to 0$, the above formula becomes the traditional Birks' formula:

$$\left.\frac{dE}{dx}\right|_{Z\to 0}\approx\frac{aZ^2}{1+cZ^2} \tag{13}$$

The calibration of light saturation is performed using the dynode signals, by minimizing the value defined as follows:

$$\sum_{i=1,Z=3}^{N_{\mathrm{pm}},Z_{\max}}\left(\frac{D_{i,Z}-\frac{G_i Z^2}{1+b\ \arctan\left(\frac{c}{b}Z^2\right)}}{\sigma_{i,Z}}\right)^2 \tag{14}$$

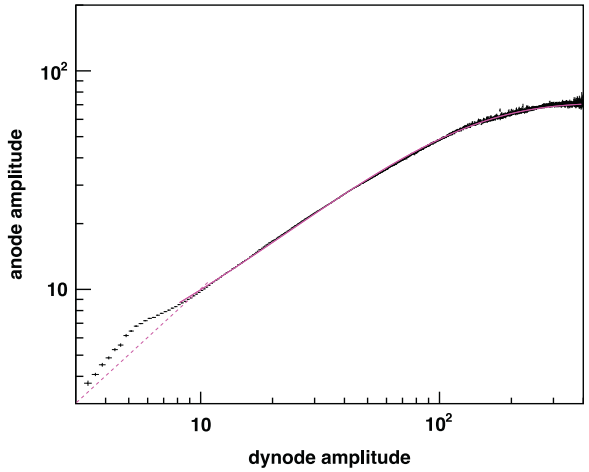

Fig. 12. Anode amplitude versus dynode amplitude. The anode high amplitude part is corrected for non-linearity using the dynode amplitude as reference (solid line), the anode low amplitude for charge measurement is extrapolated using anode linear range (dashed line).

where N_{pm} is the number of PMTs for one counter, $Z_{\max}$ is the maximum detectable charge Z, $D_{i,Z}$ is the average dynode amplitude (corrected for attenuation) for Z, b and c are the saturation parameters, G_i is the dynode gain (equivalent to the factor $G_{\mathrm{dynode,eq}}$ defined in Eq. (11)) and $\sigma_{i,Z}$ is the standard deviation of $D_{i,Z}$. The minimization procedure determines the parameters b and c for each counter.

5.3. Anode non-linearity calibration

Due to the limited dynamic range of the anode ADCs, the anode signal saturates for high charges. Fig. 12 shows the anode amplitude compared to the dynode amplitude in a large amplitude range.

In order to extend the anodes measuring range, this effect is corrected as follows:

1. determine the anode non-linearity by using the dynode amplitude as reference whenever possible;
2. extrapolate the anode measurement at lower energy deposition, where the dynode signal is not present.

For anode signal a function f_{anl} is defined, to correct the non-linear anode response(equalized for gain $G_{\mathrm{anode,eq}}$) to the dynode amplitude scale A_{AD}:

$$A_{\mathrm{AD}}=\frac{A_{\mathrm{measured}}}{G_{\mathrm{anode,eq}}\ f_{\mathrm{anl}}} \tag{15}$$

which is further equalized for attenuation:

$$A_{\mathrm{eq}}=\frac{A_{\mathrm{AD}}}{f_{\mathrm{att}}(x)} \tag{16}$$

The amplitude A_{scint} with the correction of Birks' saturation effect for each TOF counter can be obtained either from the anode measurements from the counter two sides ($A_{\mathrm{n,eq}}$ and $A_{\mathrm{p,eq}}$):

$$A_{\mathrm{anode,scint}}=f^{-1}_{\mathrm{Birks}}\left(\frac{A_{\mathrm{n,eq}}/\sigma_n^2+A_{\mathrm{p,eq}}/\sigma_p^2}{1/\sigma_n^2+1/\sigma_p^2}\right) \tag{17}$$

or from the dynode measurements weighted with the resolution of each PMT:

$$A_{\mathrm{dynode,scint}}=f^{-1}_{\mathrm{Birks}}\left(\frac{\sum_{i=1}^{N_{\mathrm{pm}}}D_{i,eq}/\sigma_i^2}{\sum_{i=1}^{N_{\mathrm{pm}}}1/\sigma_i^2}\right) \tag{18}$$

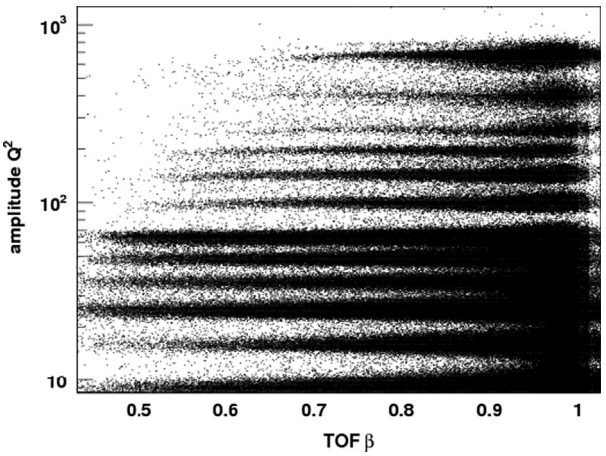

Fig. 13. TOF counter corrected amplitude as a function of β for $Z=3$ to $Z=26$.

where σ_n and σ_p are the standard deviation of the amplitude of two side anodes, $D_{i,eq}$ is the amplitude of each dynode corrected for dynode gain and attenuation, N_{pm} is the number of PMTs in each counter, σ_i is the standard deviation of the amplitude of each dynode, f^{-1}_{Birks} is the inverse of the Birks' saturation function of formula (12).

5.4. Dependence of the charge and of the energy loss from the velocity

Particle energy deposition depends on particle energy as described by the Bethe–Bloch formula ($dE/dx = f(\beta)Z^2$) [16]. Especially for the low β region, this dependence is quite significant.

The correction is based on the measured β value. However, when particle traverses the TOF paddles and the other AMS material, their velocity decreases. Consequently, different β dependences are observed for each layer and particle.

To correct the energy loss (dE/dx) from effects related to the particle energy, the following formula is used:

$$\frac{dE}{dx}\Big|_{scint} \propto A_{\mathrm{scint}} = h(\beta, A_{\mathrm{scint}})Q^2_{\mathrm{scint}} \tag{19}$$

where Q_{scint} is the counter measured charge. The function $h(\beta, A_{\mathrm{scint}})$ depends on TOF measured β and counter amplitude A_{scint}, parameterized for every counter.

Finally the continuous charge estimator Q_{scint} from each TOF counter can be derived:

$$Q_{\mathrm{scint}} = \sqrt{\frac{A_{\mathrm{scint}}}{h(\beta, A_{\mathrm{scint}})}} \tag{20}$$

Fig. 13 shows the corrected amplitude as a function of β for different Z.

5.5. Charge estimators

The charge estimator can use any or all of the charge identification capabilities: the charge can be derived from each PMT, each counter or each layer.

An overall measurement of the particle charge can be done by using the measurements at the layer level and performing a "Gaussian mean" (Q_{gaus}) with the following formula:

$$Q_{\mathrm{gaus}} = \frac{\sum_l Q_l - [Q_{\mathrm{min}} \text{ or } Q_{\mathrm{max}}]}{n-1} \tag{21}$$

where Q_l is the charge measured by layer l, Q_{max} is the maximum charge measured by any layer, Q_{min} is the minimum charge measured by any layer, and n is the number of layers. Namely,

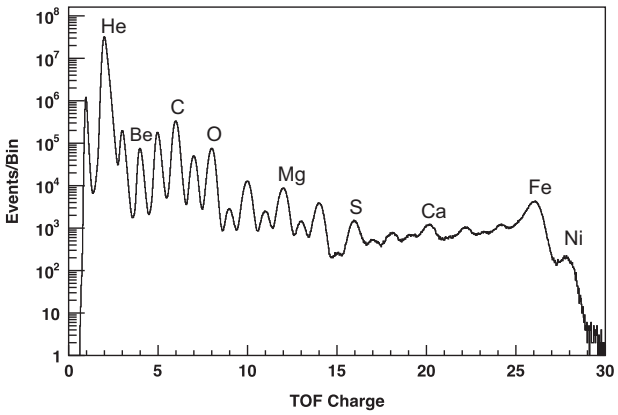

Fig. 14. TOF charge estimation for different ions obtained using the Gaussian mean calculation (Q_{gaus}, formula (21)).

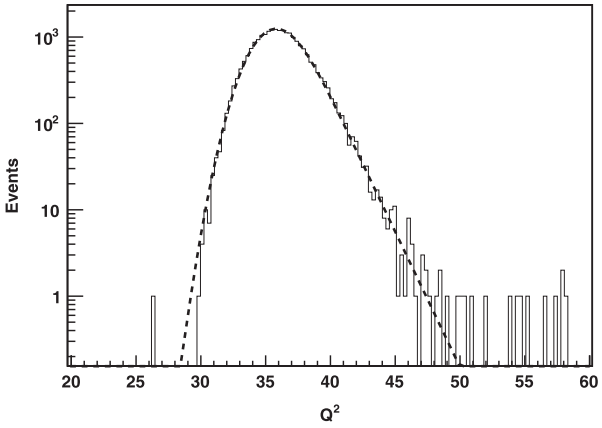

Fig. 15. Typical TOF counter amplitude (Q^2) for $Z=6$ particles. The dashed line is the related PDF function with the velocity range from 0.9 to 0.95c.

Q_{gaus} excludes the counter with the maximum deviation from average charge (the lowest or the highest) which could be used to estimate the charge of particles (see Fig. 14).

A more powerful, charge estimator uses the likelihood method to assign an integer value to the particle charge. The Likelihood charge estimator is defined as follows:

$$L(Z) = \log\left(\prod_{i=1}^{n} P_{i,Z,\beta}(Q_i)\right) \tag{22}$$

where n is the number of counters included in the measurement, $P_{i,Z,\beta}$ is the TOF charge probability density function (PDF), parameterized for each counter i, nuclei and velocity bin and Q_i is the charge estimator for counter i. An example of PDF is shown in Fig. 15 for $Z=6$ particles. PDF have been computed for particles with charge from $Z=1$ up to $Z \geq 26$.

The most probable measured charge $\hat{Z}$ is determined by solving the equation:

$$\frac{\partial L_Z}{\partial Z}\Big|_{Z=\hat{Z}} = 0$$

The probability for a given charge Z is

$$\mathrm{Prob}(Z) = \frac{\sqrt{[n]\prod_i P_{i,Z,\beta}(Q_i)}}{\sum_{Z'}\sqrt{[n]\prod_i P_{i,Z',\beta}(Q_i)}} \tag{23}$$

Prob(Z) can be used as a quality indicator for the charge measurement. In particular, if a nucleus interacts inside the AMS detector, the charge estimator in different planes will have different values and the probability Prob($\hat{Z}$) of the most probable

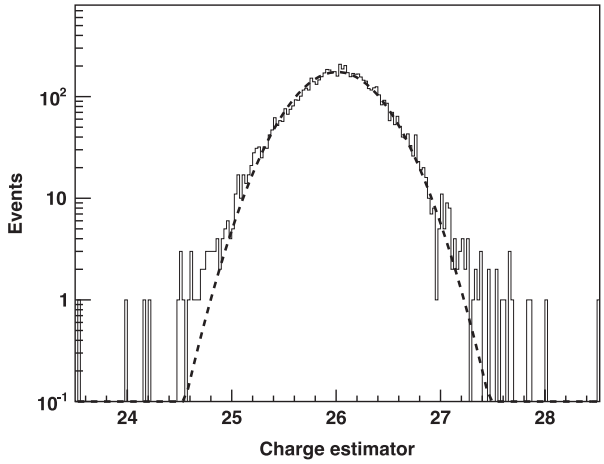

Fig. 16. Distribution of the TOF charge estimator for Iron ions ($Z=26$) for a single TOF counter. The dashed line is a Gaussian fit with standard deviation $\sigma=0.38$.

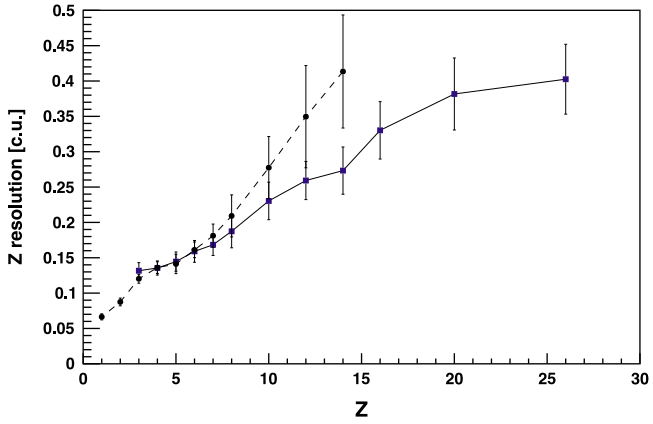

Fig. 17. Anode (dots, dashed line) and dynode (squares, solid line) charge resolution in charge units (c.u.) as a function of Z; the error bars represent the standard deviation of the distribution of resolution for all TOF counters.

charge will show a lower value with respect to non-interacting nuclei.

5.6. Performance in space

Once all the dynamic and static calibration procedures are applied, the TOF is capable of measuring all particle charges from $Z=1$ to $Z=40$ with high precision, as shown in Fig. 14. In Fig. 16 the charge resolution of a single TOF counter for Iron ions is shown. The charge resolution of a single TOF counter with respect to particle charge Z is shown in Fig. 17. Both anodes and dynodes have good resolution for charge measurement. Low charges ($1 \leq Z \leq 3$) are measured using anodes, middle charges ($4 \leq Z \leq 8$) are measured using both anodes and dynodes, and high charges ($Z > 8$) are measured using dynodes.

A single TOF counter has a charge resolution $\sim$0.16 charge unit (c.u.) for Carbon ($Z=6$) and $\sim$0.4 charge unit for Iron ($Z=26$).

6. Conclusions

The time of flight detector plays a major role in the AMS-02 experiment to study cosmic nuclei physics. Since May 2011, the TOF detector is operating in the International Space Station without problems. All the counters are working properly.

The velocity resolution ($\Delta\beta/\beta^2$) achieved in space is 4% for Proton and 1.2% for Carbon.

The measured charge resolution for one TOF counter is $\sim$0.16 charge units (c.u.) for Carbon and $\sim$0.4 charge units for Iron.

References

[1] M. Aguilar, et al., Physical Review Letters A 110 (2013) 141102.
[2] A. Kounine, International Journal of Modern Physics E 21 (2012) 123005.
[3] B. Alpat, et al., Nuclear Instruments and Methods in Physics Research Section A 613 (2010) 207.
[4] V. Bindi, et al., Nuclear Instruments and Methods in Physics Research Section A 623 (2010) 968.
[5] Th. Kirn, Nuclear Instruments and Methods in Physics Research Section A 706 (2013) 43.
[6] Ph. von Doetinchem, W. Karpinski, Th. Kirn, K. Lübelsmeyera, St. Schael, M. Wlochal, Nuclear Physics B: Proceedings Supplements 197 (2009) 15.
[7] M. Aguilar-Benitez, et al., Nuclear Instruments and Methods in Physics Research Section A 614 (2010) 237.
[8] S. Rosier-Lees, et al., Journal of Physics: Conference Series 404 (2012) 012034.
[9] Hamamatsu Photonics: Photomultipler tube R5946, 1994.
[10] L. Brocco, et al., Behavior in strong magnetic field of the photomultipliers for the TOF system of the AMS-02 space experiment, in: Proceedings of the 27th ICRC, 2001, pp. 2193–2196.
[11] G. Levi, et al., Nuclear Instruments and Methods in Physics Research Section A 530 (2004) 419.
[12] A. Basili, et al., Nuclear Instruments and Methods in Physics Research Section A 707 (2013) 99113.
[13] J. Christiansen, High Performance Time to Digital Converter, 2002.
[14] L. Gallin-Martel, et al., IEEE Transactions on Nuclear Science NS-49 (4) (2002) 1798.
[15] Alpha Magnetic Spectrometer-02. Structural Verification Plan for the Space Transportation System and the International Space Station, JSC 28792, August 2003, Rev. C document.
[16] H. Bethe, J. Ashkin, Experimental Nuclear Physics, John Wiley, NY, 1953.
[17] J.B. Birks, The Theory and Practice of Scintillation Counting, Pergamon Press, 1964.